The Impact of PMD on Single-Polarization Nonlinear Frequency Division Multiplexing

The Impact of PMD on Single-Polarization Nonlinear Frequency Division Multiplexing

Iman Tavakkolnia, *Member, IEEE,* and Majid Safari, *Member, IEEE*

***Abstract*—The impact of polarization mode dispersion (PMD) is studied on the single-polarization signal transmission over the continuous spectrum (CS) of a long-haul optical fiber link defined by nonlinear Fourier transform (NFT). It is shown that a linear all-order PMD compensation can reverse most of PMD effects in the temporal domain. However, due to the nonlinear interaction of the two polarization modes, the CS is distorted in the nonlinear spectral domain. Simulation results are presented, and a perturbation model is proposed based on the simulation results to describe the impact of PMD for different modulation formats and fiber parameters. It is demonstrated that, after linear PMD compensation, the residual polarization-dependent effects generate a constellation rotation and additional noise in the nonlinear spectral domain. The performance of NFT-based system in the presence of both PMD and amplifier noise is also studied. The results show that the effect of PMD is small provided that an efficient linear PMD compensation is performed in time domain.**

***Index Terms*—Optical fiber communication, nonlinear Fourier transform, polarization mode dispersion, continuous spectrum.**

I. Introduction

The nonlinear Fourier transform (NFT) is regarded as a potential solution to the fiber nonlinearity problem, which is the main origin of data rate limitation in long-haul optical fiber communication [1]–[3]. The NFT transforms the nonlinear propagation of temporal signal, governed by the nonlinear Schrödinger equation (NLSE), into simple linear evolution of continuous and discrete spectra in the so-called nonlinear spectral domain [4]–[6]. These spectra and the corresponding nonlinear spectral domain, defined by the NFT, are the generalized counterparts of the linear spectrum and frequency domain defined by the ordinary Fourier transform. Using the NFT, the optical fiber channel is effectively linearised, and the basic idea is to utilize degrees of freedom in the nonlinear spectral domain for data transmission [7]. However, many aspects of this concept require rigorous investigation due to complexity and infancy of the approach [2].

In NFT-based optical communication, systems can be defined based on data transmission over the continuous spectrum (CS) [8], [9], the discrete spectrum (DS) [10]–[13] or both spectra [14]–[16]. Signalling on the CS is an attractive approach since the CS basically consists of a continuous complex waveform, and thus many known conventional communication techniques can be applied. High data rates have already been demonstrated for the CS by simulation and experiment [17], [18]. The capacity of such communication system is studied [19], [20], the computational complexity and essential practical considerations are investigated [21], [22], and many performance improvement techniques are proposed [23]–[26]. Recently, dual polarization NFT-based systems for CS [27], [28] and DS [29], [30] were proposed, and new forms of NFT were defined based on the Manakov equation. Nevertheless, most of the current literature focuses on single polarization NFT-based systems where the NFT is originally defined based on the scalar NLSE. Therefore, a major assumption is needed in the definition of NFT, which is the absence of randomly varying birefringence and polarization mode dispersion (PMD). Nevertheless, this is usually not a practical assumption specifically in long-haul optical fiber systems, where fibers are subject to unavoidable environmental stress (e.g., pressure on fibers laid on the sea bed). Even in dual polarization systems [27]–[31], the random effect of PMD should be studied separately. In [32], the perturbative effect of PMD was briefly studied and the nonlinear frequency division multiplexing (NFDM) was compared with the wavelength division multiplexing (WDM). It was stated that the achievable information rates for WDM and NFDM are almost equal including the effects of PMD and higher order dispersion.

In this paper, the effect of PMD on the CS is studied for a single-polarization NFT-based transmission system. Generally, in high-speed coherent optical communication systems, some treatment of PMD effects is essential. Due to the lack of an optimal PMD compensation method in the presence of nonlinearity, the all-order linear PMD compensation method is opted here. Simulation results show that such a PMD compensation is effective and can reverse most of the distortion caused by PMD in temporal domain. Then, the impact of the remaining uncompensated effects of PMD on CS, as a consequence of nonlinear interaction between the polarization modes, are examined. It is observed from simulation results that the main impact of the residual polarization-dependent effect includes a signal-dependent phase shift and a noise-like error. Similar effects were also reported in [27] for dual-polarization NFT-based systems. An analytical framework is also provided based on simulation results to model the impact of PMD after linear compensation. It is demonstrated that, apart from the PMD parameter, the fiber length, input power, and instantaneous signal amplitudes are the parameters that can be used to describe the residual perturbation caused by PMD. Our results show that, an effective linear PMD compensation in time domain makes the distortion caused by PMD negligible in most cases. Finally, the combined effects of PMD and amplified spontaneous emission (ASE) noise are

Manuscript received X; revised X.

Authors are with the Institute for Digital Communications, School of Engineering, University of Edinburgh, Edinburgh, EH9 3FD, UK. e-mail:{i.tavakkolnia, majid.safari}@ed.ac.uk

evaluated.

The paper is presented as follows. In Section II, the NLSE, the definition of NFT and the channel model for CS are reviewed. The temporal channel model in the presence of PMD is explained in Section III. The effect of PMD is studied in Section IV, and numerical results are presented in Section V for different PMD parameters, link lengths, and signal powers. A brief abstract of this work was published in [33].

II. System model

In this section, we briefly review the system model for the basic single-polarization communication system that uses the CS of nonlinear optical fiber for data transmission by ignoring polarization effects. In the next sections, the effect of randomly varying polarization state and PMD will be investigated.

Most of the proposed NFT-based systems are defined based on the assumption that the optical signal is transmitted in a single polarization, the polarization state does not change along the fiber, and the PMD is negligible. Therefore, a scaler channel model without PMD is used. In such an ideal condition, the propagation of the optical field in a single polarization in a standard single-mode fiber can be described by the well-known scaler stochastic nonlinear Schrödinger equation (NLSE) [34]. The NLSE is the model widely used in optical fiber communication and is also regarded as an accurate model for simulating optical fiber links. We assume that the fiber loss is compensated using an ideal distributed amplification system. Thus, the NLSE is described as

$$\begin{aligned}\frac{\partial Q(T,l)}{\partial l} =& -\frac{j\beta_2}{2}\frac{\partial^2 Q(T,l)}{\partial T^2} + j\gamma Q(T,l)\,|Q(T,l)|^2 \\ &+ N(T,l),\ \ 0 \le l \le L,\end{aligned} \tag{1}$$

where $Q(T,l)$, l, and T respectively represent the complex envelope of the optical field, distance, and time. $N(T,l)$ represents the ASE noise added by the amplifiers which is a white Gaussian process [34], [35]. Throughout this paper, we consider the focusing case $\beta_2 < 0$ without any kind of dispersion compensation. The NLSE (1) can be normalized in the form of

$$j\frac{\partial q(t,z)}{\partial z} = \frac{\partial^2 q(t,z)}{\partial t^2} + 2|q(t,z)|^2 q(t,z) + n(t,z), \tag{2}$$

by normalization rules

$$q = \sqrt{\gamma T_0^2/|\beta_2|}Q, \quad z = \frac{|\beta_2|l}{2T_0^2}, \quad t = \frac{T}{T_0}, \tag{3}$$

where T_0 is the normalization parameter that is considered equal to 0.25 ns throughout this paper.

The NFT is defined based on (2), and the time domain optical signal is transformed into scattering data which evolve linearly along the fiber in nonlinear spectral domain [36]. The CS, represented as $\rho(\lambda, z)$, is defined on the real axis $\lambda \in \mathbb{R}$, and can be obtained by solving the so-called Zakharov-Shabat eigenvalue problem [37]. It can be shown that, in a noise-free scenario, eigenvalues are preserved during the evolution along the fiber, and the nonlinear fiber only imposes an exponential

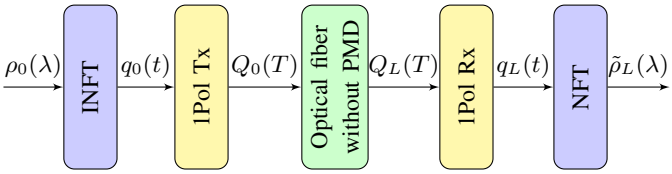

Fig. 1: Block Diagram of a single-polarization NFT-based system without PMD.

transfer function on the continuous and discrete spectra [36]. For CS, the evolution equation is expressed as

$$\rho(\lambda, z) = \rho(\lambda, 0)e^{-4j\lambda^2 z}. \tag{4}$$

There exist several fast and efficient numerical methods in the literature for NFT and INFT operations [38]–[42]. We use the Ablowitz method for NFT and discretization of Marchenko equations to implement INFT operation [14]. The split-step Fourier method is applied for simulating the propagation of signal along the fiber. More details about our simulation method can be found in [20].

As stated earlier, in this paper, we consider the signalling only on the CS, which corresponds to dispersive radiation waves. In other words, solitonic waves are not studied throughout this paper. For simplicity in notation, the dependence to the distance is dropped and shown as a subscript. In Fig. 1, $\rho_0(\lambda)$ is the input CS signal which is derived by applying a raised-cosine filter to the vector containing the modulated data symbols. Then, INFT is applied to generate the time domain signal $q_0(t)$. The single-polarization optical transmitter (1Pol Tx) launches the signal into the fiber after all required operations, such as normalization in (3), optical filtering, and digital-to-analog conversion. The signal is propagated along a standard single mode fiber without considering the PMD. Ideal distributed amplification is assumed. The signal is detected by a single-polarization optical receiver (1Pol Rx), and necessary operations are performed to capture the digital time domain signal $q_L(t)$. Then, NFT is applied, the phase shift introduced according to (4) is removed, and the noisy CS signal $\tilde{\rho}_L(\lambda)$ is obtained. Using perturbation theory and numerical simulation [19], [20], it has been shown that the channel model in the nonlinear spectral domain can be expressed as

$$\tilde{\rho}_L(\lambda) = \rho_0(\lambda) + \eta_L(\lambda, \rho_0(\lambda)), \tag{5}$$

where $\eta_L(\cdot)$ is generally a complex non-Gaussian noise with a signal-dependent variance. The noise samples can be assumed uncorrelated when the symbols are distant enough in nonlinear frequency domain. More details along with the distribution of $\eta_L(\cdot)$ is presented in [20].

III. Fiber propagation model with PMD

Two orthogonally polarized modes (e.g., x and y) can travel through the single mode fiber at the same time. These modes are degenerate in the sense that their refractive indexes are identical as long as the fiber is perfectly cylindrical and free from environmental stress. In realistic conditions, fiber is subject to imperfections and random effects which violate the ideal condition of perfect symmetry. This causes random variation of the propagation constants (or refractive indexes)

as well as the orientation of two orthogonally polarized modes along the fiber. Consequently, the fields in the two polarization states would randomly interact as the light propagates down the fiber. The accumulated effect of random birefringence in fiber leads to pulse broadening which is referred to as PMD.

In order to model the effects of random birefringence and PMD on a propagating signal [34], [43], [44], the fiber is split into segments of correlation length l_c having constant birefringence while the birefringence orientation randomly varies from one segment to another. The optical signal propagation within each of those segments with fixed birefringence can be described by the coupled nonlinear Schrödinger equations (CNLSE) as [43], [45]

$$\frac{\partial U}{\partial l} = -\frac{1}{2}\Delta\beta_1\frac{\partial U}{\partial T} - j\frac{1}{2}\beta_2\frac{\partial^2 U}{\partial T^2} + j\gamma\left(|U|^2 + \frac{2}{3}|V|^2\right)U, \tag{6a}$$

$$\frac{\partial V}{\partial l} = +\frac{1}{2}\Delta\beta_1\frac{\partial V}{\partial T} - j\frac{1}{2}\beta_2\frac{\partial^2 V}{\partial T^2} + j\gamma\left(|V|^2 + \frac{2}{3}|U|^2\right)V, \tag{6b}$$

where $U \equiv U(T,l)$ and $V \equiv V(T,l)$ are slowly varying complex envelopes of optical fields in the two orthogonal linear polarizations aligned with the orientation of birefringence. Note that the CNLSE in (6) are derived for the practical physical case of small beat length compared to the other length scales (i.e., nonlinearity, chromatic dispersion, and polarization induced differential group delay). For this case, the effect of rapid variations due to the birefringent beating is cancelled out by averaging over the rapidly varying term (containing $\exp(\pm\Delta\beta_0 l)$) [45]. This condition is almost always satisfied for practical scenarios of optical fiber communication.

In (6), the terms including $\Delta\beta_1$ is responsible for the effect of *linear birefringence*, where $\Delta\beta_1$ is the inverse group velocity difference between the two polarization modes. Other additional terms in (6) with respect to (1) are nonlinear terms with the factor 2/3, which describe the cross-phase modulation (XPM) between the two polarization modes. The XPM terms induce nonlinear coupling between the polarization modes leading to a *nonlinear birefringence* effect. Note that in the absence of PMD (i.e., $\Delta\beta_1 = 0$) and assuming single polarization transmission (i.e., $U(T,0) = Q(T,0)$ and $V(T,0) = 0$), the CNLSE in (6) reduces to the scalar NLSE in (1) and thus the two effects indicated above would not be present.

In order to model the variation of the birefringence orientation along the fiber, the optical fields are rotated randomly at the end of each segment by a unitary complex rotation matrix

$$\mathbf{R} = \begin{pmatrix} \cos(\theta) & \sin(\theta)e^{j\phi} \\ -\sin(\theta)e^{-j\phi} & \cos(\theta) \end{pmatrix} \tag{7}$$

where $-\pi \le \theta \le \pi$ and $-\pi/2 \le \phi \le \pi/2$ are uniform random variables, representing an arbitrary rotation on the Poincare sphere with random geometrical rotation θ and random phase difference ϕ between U and V [43], [44]. Note that in the presence of PMD, even if the initial signal is polarized in one of the orthogonal polarization states, part of the energy is coupled to the other polarization state during the propagation due to linear and nonlinear birefringence as well as the randomly varying orientation of birefrngence.

IV. Effects of PMD on the CS

The single-polarization NFT is defined based on nonlinear fiber propagation while neglecting the PMD effect, and this is an inherent assumption in most of the current research on the NFT-based systems. Here, we intend to evaluate the degrading effects of PMD on such NFT-based systems, focusing on the signalling over CS. Based on (6), for signal-polarization transmission even if the signal is initially aligned with one of the orthogonal polarizations of the fiber, a significant portion of the energy is coupled to the other polarization mode after propagation over a long link due to PMD. Therefore, in order to achieve an effective signal detection using single-polarization NFT, first some form of PMD compensation is required to return most of the signal energy to the original polarization state.

For linear scenarios, several optical compensation techniques are proposed which basically require determining the principal polarization states of the fiber and applying a fixed or variable delay between them in one or multiple stages thereby compensating PMD to the first or higher orders [46]–[48]. Electronic equalization techniques can provide similar performances while enabling a low-complexity design. However, there is no systematic method to take into account the effect of nonlinearity in the compensation of PMD effects [45]. Therefore, here, we use an ideal linear PMD compensation technique that can adaptively mitigate all orders of PMD effect in the absence of fiber nonlinearity. It should be mentioned that we expect such a linear all-order PMD compensation method to work reasonably well for the CS because, in the absence of soliton component, the large dispersion would push the system to a nearly linear regime after an initial link distance.

A. Linear all-order PMD compensation

In the linear regime, the effect of PMD in the fiber is modelled as the concatenation of randomly oriented birefringent segments and can be represented as frequency dependent unitary Jones matrices as [34], [46]

$$\mathbf{A}(\omega) = \prod_{k=1}^{K} \mathbf{A}_k(\omega), \tag{8}$$

where

$$\mathbf{A}_k(\omega) = \begin{pmatrix} e^{i\omega\Delta\beta_{1k}l_c/2} & 0 \\ 0 & e^{-i\omega\Delta\beta_{1k}l_c/2} \end{pmatrix} \begin{pmatrix} \cos(\theta_k) & \sin(\theta_k)e^{j\phi_k} \\ -\sin(\theta_k)e^{-j\phi_k} & \cos(\theta_k) \end{pmatrix}, \tag{9}$$

and $\Delta\beta_{1k}$ is the inverse group velocity in kth segment. Note that, in the absence of nonlinearity ($\gamma = 0$ in (6)), the first term in the right hand side of (9) simply models linear propagation in a segment of fiber with fixed birefringence. Therefore, the linear effect of PMD can be fully mitigated by applying $\mathbf{A}^{-1}(\omega)$ to the received field [46]. This is called all-order PMD compensation and requires channel state information or, in other words, the matrix $\mathbf{A}(\omega)$ at every frequency. Although the linear all-order PMD compensation would essentially eliminate the PMD effect in the linear regime, it cannot reverse

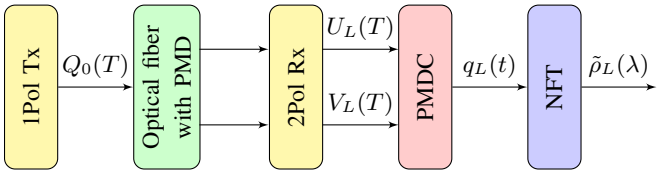

Fig. 2: Block Diagram of a single-polarization NFT-based system with PMD compensation.

the interaction of PMD with nonlinearity when such an effect is significant.

To apply the linear all-order PMD compensation described above to the NFT-based communication system, a dual polarization coherent optical receiver is required as shown in Fig. 2 where the PMD compensation is performed digitally using the PMD compensation (PMDC) block as

$$\begin{pmatrix}\hat{U}_L(\omega)\\ \hat{V}_L(\omega)\end{pmatrix} = \mathbf{A}^{-1}(\omega)\begin{pmatrix}U_L(\omega)\\ V_L(\omega)\end{pmatrix} \tag{10}$$

where $U_L(\omega)$ and $V_L(\omega)$ are the fields in frequency domain. It is assumed that the matrix $\mathbf{A}(\omega)$ is fully known at the receiver through estimation based on a training sequence. Assuming that the input optical signal is linearly polarized in the x direction, the output of PMDC block $q_L(t)$ is given as $\hat{U}_L(T) = \text{IFFT}[\hat{U}_L(\omega)]$ normalized by (3). Note that the fiber propagation with PMD, in Fig. 2, is described by (6), where $U_0(T) = Q_0(T)$ and $V_0(T) = 0$. The rest of the system is identical to conventional structure in Fig. 1. Using the relationship $D_P = \Delta\beta_1\sqrt{8l_c/3\pi}$ to determine the average value of $\Delta\beta_1$ [43], the received signal at the output of different blocks in Fig. 2 can be generated as shown in Figs. 3a and 3b. For this simulation, the transmission of a 16QAM modulated CS signal over the length of $L = 2000$ km of fiber with PMD parameter $D_P = 0.4$ ps/$\sqrt{\text{km}}$ is assumed. Throughout this paper, symbols are modulated on 64 "subcarriers" of CS in nonlinear frequency domain [16], [20]. Raised-cosine filter is used to generate the continuous waveform containing the data symbols. The signal bandwidth is 52 GHz and the baud rate is 20 Gbuad. The parameter $\Delta\beta_1$ is random and assumed to be normally distributed. The correlation length is $l_c = 100$ m.

During the propagation of signal along the fiber, birefringence causes the signal energy to transfer from one polarization state to the other. Hence part of the signal energy would be coupled into the non-original polarization state, as shown in Fig. 3a. In fact, before any PMD compensation, each of the two received polarization components contain almost half of the signal energy for sufficiently long fibers. Then, by applying the linear all-order PMD compensation, most of the signal energy is recovered at the original polarization state, and only a small portion of the energy remains in the other polarization state due to the nonlinear interaction between the two polarizations, as observed in Fig. 3b. This residual polarization-dependent distortion can be seen also after NFT as in Fig. 3c where the recovered CS is slightly distorted. This affects the detection of transmitted bits modulated on CS. In order to characterize this residual effect, in the next subsection, we first investigate the transmission of signals with single or multi-level constellations in the absence of noise.

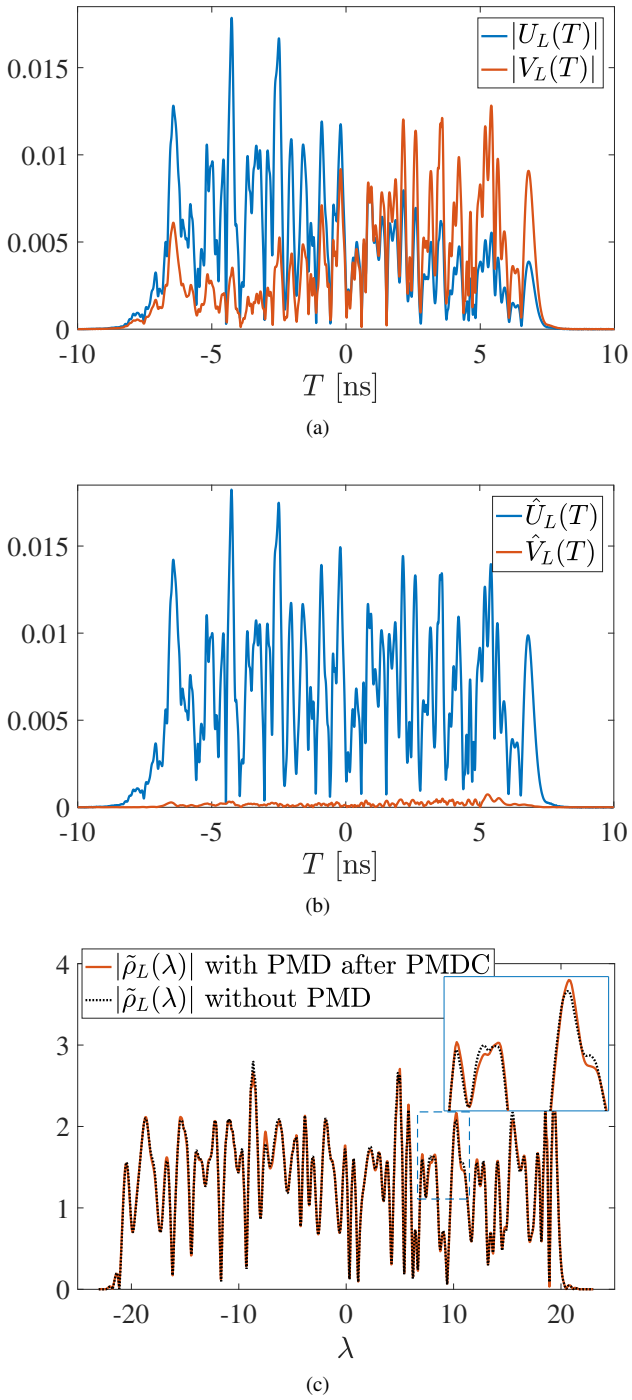

Fig. 3: (a) Received signals in two polarization before PMDC. (b) Signals in two polarizations after PMDC. (c) CS after PMDC in comparison to PMD-free case.

In this paper we use the error vector magnitude (EVM) to evaluate the performance degradation in the presence of ASE noise or PMD, which is defined as

$$\text{EVM} = \frac{\sqrt{\frac{1}{I}\sum_{i=1}^{I}|s_L^i - s_0^i|^2}}{|s_0^{\max}|} \tag{11}$$

for total number of simulation samples I. Here, s_0^i and

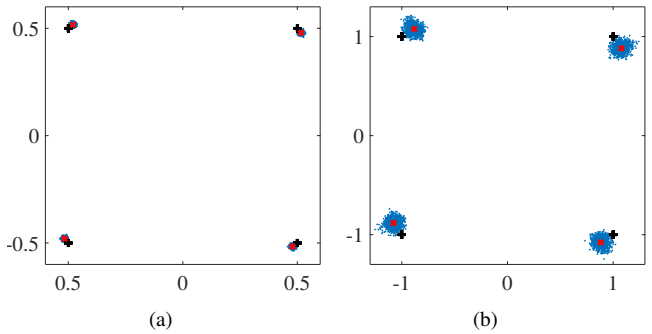

Fig. 4: Detected symbols after PMDC and NFT operation for QPSK modulation at launch powers (a) -9 dBm and (b) -6 dBm. Blue dots are the detected symbols, black pluses are the original symbols, and red crosses are mean values of detected symbols.

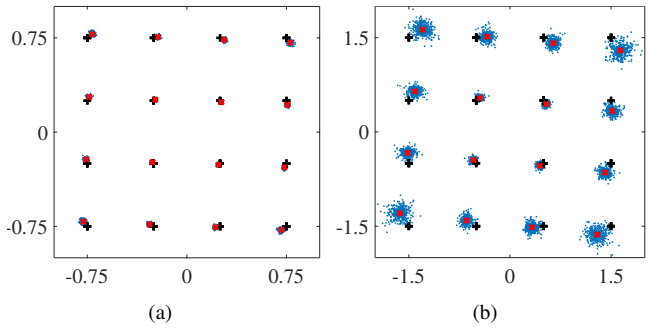

Fig. 5: Detected symbols after PMDC and NFT operation for 16QAM modulation at launch powers (a) -9 dBm and (b) -6 dBm. Blue dots are the detected symbols, black pluses are the original symbols, and red crosses are mean values of detected symbols.

s_L^i respectively represent the ith transmitted and received symbols. In (11), $|s_0^{\max}|$ is the maximum symbol amplitude in the constellation.

B. Single- and multi-level signalling in the presence of PMD

Here, we evaluate the performance of the NFT-based communication system in Fig. 2 after linear all-order PMD compensation considering single- and multi-level modulations. In order to elucidate the impact of PMD, a noise-free case ($n(t,z)=0$) is initially considered.

First, the transmission of a QPSK signal is simulated at two different launch powers with channel parameters the same as before (i.e., $D_P = 0.4$ ps/$\sqrt{\text{km}}$ and $L = 2000$). The received symbols after propagation along the fiber and experiencing nonlinearity and random birefringence are demonstrated in Fig. 4. Note that linear all-order PMD compensation is already applied at the receiver. The results clearly show that the constellation diagram is rotated, and symbols are received with random errors. Moreover, both effects of rotation and random errors increase at higher launch power. Fig. 5 shows the received symbols after 2000 km of fiber length with PMD parameter $D_P = 0.4$ ps/$\sqrt{\text{km}}$ for a 16QAM modulation format. It is observed that similar to the QPSK format, the residual polarization-dependent effect depends on the launch power. Also, it can be seen that the rotation angle of the constellation diagram and noise cloud size depend on the symbol amplitude as well as launch power. Note that similar effects were also reported in [27] in dual-polarization NFT-based system, where PMD effects were compensated by a linear training sequence based equalization algorithm.

Table I reports the average EVM and average rotation angle (shown by ψ) of the constellation diagram for the QPSK modulation. It is observed that both quantities increase for larger values of power and fiber length. Thus, the residual polarization-dependent nonlinear effect on CS in single-level modulation can be described as a power and distance dependent phase shift and a contribution to the additive signal dependent noise in CS.

Following the observation in Fig. 5 that the nonlinear polarization-dependent perturbation not only depends on signal power but also on the signal amplitude, the average EVM and average rotation angles of constellation are calculated for three different symbol amplitudes in 16QAM modulation format. For such a modulation format, rings with constant amplitude are shown by r_j for $j = 1, 2, 3$. The definition of EVM for each ring is

$$\text{EVM}^j = \frac{\sqrt{\frac{1}{I_j}\sum_{i=1}^{I_j} |s_L^{ij} - s_0^{ij}|^2}}{|s_0^{\max}|} \tag{12}$$

where I_j is the total number of the simulation samples for corresponding ring j. The results presented in Table II, confirm that both perturbation effects (i.e., constellation rotation and random error) directly depend on the symbol amplitude as well as average power and fiber length although the dependence of the rotation angle to signal amplitude is not as strong as other dependencies.

TABLE I: The average EVM and average rotation angle of the constellation ψ for QPSK modulation format with launch powers -9 and -6 dBm for $D_P = 0.4$ ps/$\sqrt{\text{km}}$.

	$L = 1000$ [km]		$L = 2000$ [km]	
P [dBm]	ψ [Rad]	EVM [%]	ψ [Rad]	EVM [%]
-9	0.0306	3.18	0.0387	3.99
-6	0.0812	8.55	0.1026	10.77

C. Modified NLSE perturbed by the residual polarization-dependent effect

In the absence of nonlinearity, the linear all-order PMD compensation in Fig. 2 perfectly reverses effects of PMD. However, when the nonlinearity is not negligible some polarization-dependent effects remain uncompensated. This residual effect is caused by the cross-phase modulation defined by (6) which is not taken into account in the linear PMD compensation as well as the random birefringence along the fiber. Note that, for larger D_P and thus larger $\Delta\beta_1$, the signal's degree of polarization degrades more quickly due to the increased linear birefringence and this may further reinforce the nonlinear interaction defined by the XPM terms in (6) as observed in the results of the next section. As indicated before, the use of the linear PMD compensator allows for the application single-polarization NFT defined by

TABLE II: The average EVM and average rotation angle ψ for 16QAM modulation format with launch powers -9 and -6 dBm for $D_P = 0.4$ ps/$\sqrt{\text{km}}$ and $L = 2000$ km.

P [dBm]	ψ [Rad]			EVM^j [%]		
	r_1	r_2	r_3	r_1	r_2	r_3
-9	0.0424	0.0442	0.0466	1.55	3.41	4.8
-6	0.1004	0.1093	0.1178	3.61	8.5	12.45

scalar NLSE. Therefore, the NFT-based transmission system after linear PMD compensation can be still modelled by the scalar NLSE while additionally perturbed by the residual polarization-dependent effects described above. As a result, we consider a modified NLSE given by

$$j\frac{\partial q(t,z)}{\partial z} = \frac{\partial^2 q(t,z)}{\partial t^2} + 2|q(t,z)|^2 q(t,z) + n(t,z) + h(t,z), \tag{13}$$

where $h(t,z)$ is the additional perturbation term representing the residual polarization-dependent effect. Note that the proposed model in (13) is a general perturbation model for the NLSE, which is a common approach in modeling the effect of distortions that make the NLSE deviating from its ideal form.

Based on the simulation results presented in the last subsection, we can characterize the residual polarization-dependent effect as the combination of a deterministic effect, i.e., the average rotation of constellation points and a random effect, i.e., the random error cloud around the average constellation points. Results in Tables I and II show that the impact of the polarization-dependent perturbation, $h(t,z)$, depends on both the fiber length as well as the signal amplitude. Therefore, $h(t,z)$ can be generally modelled as

$$h(t,z) = G(q(t,z)) + e(t,z). \tag{14}$$

where the deterministic signal-dependent function $G(q(z,t))$ models the average rotation of constellation points while $e(t,z)$ represents the zero-mean noise-like random error after linear PMD compensation. Therefore, $G(q(t,z)) = \mathsf{E}_q\{h(q(t,z))\}$ manifests the average perturbation effect over different signals in time while $e(t,z)$ describes the fluctuations around this average which depends on the actual realizations of the signal.

Now, let us first focus on the special case of single level modulation (i.e., all symbols have the same amplitude, such as QPSK) where results in Fig. 4 and table I shows a fixed rotation angle for all the constellation points and random error around them with the same cloud size. While the rotation angle or error cloud size are fixed across different constellation points, they increase by increasing the launch power or link length. Note that based on our results in Table I, the statistics of $e(t,z)$ in CS (after NFT operation) is signal dependent, which is similar to the effect of ASE noise after NFT transformation as investigated in [20]. Therefore, the term $e(t,z)$ is modelled as a statistically independent noise term that can be merged into the original noise term as $n'(t,z) = n(t,z) + e(t,z)$. On the other hand, the generic function $G(q(t,z))$ should represent the effect of the constant constellation rotation averaged over different single-level modulated signals and can be thus replaced by the simpler form, $G(q(t,z)) = P(z)q(t,z)$, as we will explain next. Therefore, the proposed deterministic perturbed NLSE (i.e., disregarding ASE noise $n(t,z)$ and error $e(t,z)$) is expressed as

$$j\frac{\partial q(t,z)}{\partial z} = \frac{\partial^2 q(t,z)}{\partial t^2} + 2[|q(t,z)|^2 + \frac{1}{2}P(z)]q(t,z), \tag{15}$$

which is in the same form as the NLSE that describes the propagation of electromagnetic waves in an inhomogeneous plasma. In [49], it was shown that for a real function $P(z)$, the inverse scattering method holds for solving (15) without major modifications. Therefore, after a simple manipulation of Zakharov-Shabat eigenvalue problem and the corresponding evolution problem, the evolution of CS can be derived as [36], [49]

$$\rho_L(\lambda) = \rho_0(\lambda)e^{-4i\lambda^2 z + \psi(z)}, \tag{16}$$

where

$$\psi(z) = -i\int_0^z P(\zeta)\mathrm{d}\zeta, \tag{17}$$

denotes the average phase shift defining the constant rotation of the different constellation points in single-level modulation as observed in our results. The equality in (17) confirms that the average phase shift introduced in the solution of the modified NLSE is expressed in terms of the integral of the function $P(z)$ which should be a real function of the fiber length, PMD parameter, and signal power[1] as expected for single-level modulation based on the results of the last subsection. Consequently, when noise and the residual random error (i.e., $n'(t,z) = n(t,z)+e(t,z)$) are included, the solution of the modified NLSE after linear dispersion compensation (i.e., removing $e^{-4i\lambda^2 z}$ according to (4)) can be expressed as

$$\tilde{\rho}_L(\lambda) = \rho_0(\lambda)e^{\psi(z)} + \eta'_L(\lambda, \rho_0(\lambda)), \tag{18}$$

where $\eta'_L(\cdot)$ describes the combined effect of noise and error in the nonlinear spectral domain which is signal dependent as discussed in [20] [2]. Therefore, the solution of the proposed modified NLSE given by (18) characterizes the residual polarization-dependent effect as observed in our simulation results for single level modulation. Note that the dependency of $P(z)$ to the parameters of the fiber communication system can be investigated via numerical simulations, which will be the subject of future research.

In the perturbation model presented for single level modulation, the generic term $G(q(t,z))$ was simplified as $P(z)q(t,z)$ to describe the constant average rotation of different constellation points where the perturbation only depends on the signal power, PMD parameter, and the link length. On the other hand, while the simulation results for multi-level modulation show similar behaviour as in single-level modulation but they also indicate that the constellation point rotation (i.e., phase shift) is not necessarily constant across different amplitude levels

[1]Note that the perturbation term, $h(t,z)$, is a function of the signal realizations in time rather than its statistics (e.g., signal power). However, the statistics of $h(t,z)$, including $G(q(t,z)) = \mathsf{E}_q\{h(q(t,z))\}$ or $P(z)$ can be related to the signal power.

[2]It can be analytically shown that in asymptotic scenario the variance of noise in nonlinear frequency domain is explained by [20, Eq. 17] demonstrating its dependency on the instantaneous signal amplitude $|\rho_0|$ as well as fiber length z.

(i.e., rings). Nevertheless, by inspecting Table II, we can see that the dependence of the rotation angle on the amplitude of the constellation points (or ring number) is not as significant as its dependence to link length or signal power. We therefore propose that the modified NLSE in (15) can be used to approximately describe the propagation of multi-level signals along the fiber as well. Note that the inclusion of the term $e(t, z)$ as an independent noise term in time can describe the significant dependence of random error strength on individual symbol amplitudes as shown in Table II. In conclusion, the model proposed based on the modified NLSE in (15) characterizes the behaviour of the NFT-based communication system in the presence of residual polarization-dependent effect for single-level modulation accurately and for multi-level modulation approximately.

D. Constellation rotation precompensation at transmitter

In previous subsections, it was demonstrated that, after the all-order linear PMD compensation, the CS signal is affected by a constellation rotation as well as a noise-like error as a result of the residual polarization-dependent effect. The error part is combined with the ASE noise and will be investigated in the next section. The average constellation rotation is not a fundamental distortion and can be dealt with at the transmitter or receiver side. It can be estimated for any communication link before data transmission because it only depends on the constant PMD parameter associated to the particular link, modulation format, and transmission system parameters. Although the decision boundaries can be modified with Maximum-Likelihood detection at the receiver, a simpler way is to precompensate such an effect by rotating the constellation at the transmitter in reverse with proper angles at each symbol amplitude. Later, in section V, the combined effects of ASE noise and PMD are studied with the assumption that the required information is available and such precompensation is conducted at the transmitter. The study of achievable spectral efficiency in the presence of PMD with optimal detection schemes will be considered in future research.

V. Numerical analysis

In this section, the performance of single polarization NFT-based communication systems is investigated in the presence of PMD as a function of the fiber length and the PMD parameter in the absence or presence of ASE noise.

It was demonstrated in previous section that larger launch power leads to an increase in the residual polarization-dependent effect due to higher nonlinearity. Likewise, it is expected that PMD effects on the CS channel are more severe for longer fiber length or larger PMD parameter. This is investigated here by simulation. The 16QAM modulation format and -6dBm launch power is assumed while fiber length and PMD parameter vary. The average rotation angle of the constellation points and EVM (average on all amplitudes) are measured. The results are demonstrated in Figs. 6 and 7, where it is confirmed that the average value for both EVM and ψ increases for longer fiber or larger D_P. Note that for

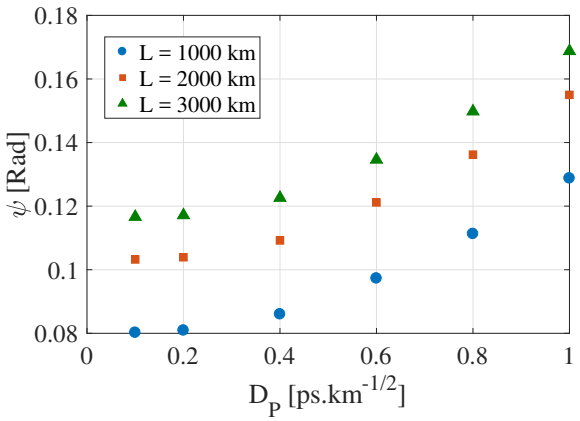

Fig. 6: Average rotation angle for different fiber lengths and PMD parameters for 16QAM modulation and -6dBm launch power.

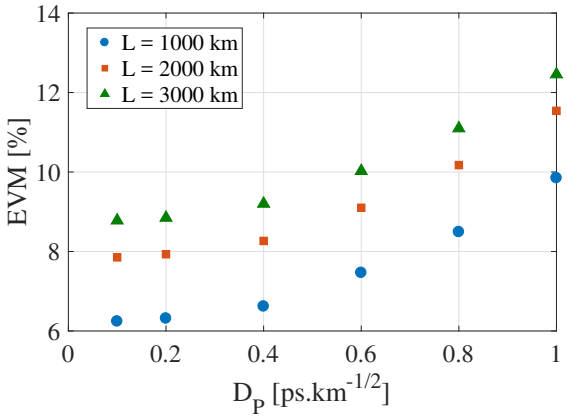

Fig. 7: Average EVM for different fiber lengths and PMD parameters for 16QAM modulation and -6dBm launch power.

simulations in this paper a CS signal containing 64 randomly modulated symbols is transmitted through the fiber 100 times separately with random independent signal and noise realizations [16], [20]. In other words, 6400 samples are used for each measurement. Note that we assume the system model in Fig. 2 which includes a linear PMD compensation, and the constellation rotation is not compensated when calculating EVM in Fig. 7.

It is observed that EVM and ψ follow similar trends. An interesting observation is that the difference between the 1000-km link and 2000-km link is larger than the difference between the 2000-km and 3000-km links. This effect can be explained by taking into account the effect of the chromatic dispersion. As the fiber length grows, the signal in time domain is dispersed more, and its amplitude is reduced. As a consequence, the impact of nonlinearity is smaller. In other words, it may be expected that the residual polarization-dependent effect does not increase after an asymptotically long fiber length when linear all-order PMD compensation is used.

The effect of PMD on the CS signal was studied in previous sections without including the ASE noise. The average rotation of the constellation diagram can be compensated by pre-compensating at the transmitter for fixed link parameters as

TABLE III: Average EVM after pre-compensation for different fiber lengths L [km] and launch power P_{in} [dBm].

		Sampling			Filtering		
P_{in}	L	PMD	ASE	ASE+PMD	PMD	ASE	ASE+PMD
	1000	0.83	9.97	10.22	0.81	4.21	4.31
-9	2000	0.95	17.3	17.54	0.92	6.09	6.14
	3000	1.01	24.77	25.36	0.98	8.82	9.04
	1000	2.73	11.41	11.85	2.53	4.37	5.09
-6	2000	3.14	20.96	21.97	2.93	6.46	7.19
	3000	3.33	31.96	33.43	3.08	10.86	11.63

the average rotation angle can be assumed to be known or estimated in a NFT-based optical fiber communication system. Here, in the second simulation in this section, we assume that such information is available, and the rotation of constellation diagram is compensated at the transmitter. We intend to study the combined effects of ASE noise and PMD by measuring the average EVM by simulation. Obviously the performance is degraded in case the average rotation angles are unknown and pre-compensation is impossible. Again, $D_P = 0.4\ \mathrm{ps}/\sqrt{\mathrm{km}}$ is considered as the PMD parameter of optical fiber. Apart from sampling the CS for detection, the performance with the linear filtering method, introduced in [8], is also presented, which is expected to improve the performance. For the linear filtering method, 18 samples per symbol are calculated by NFT.

Results are presented in Table III for three scenarios: "PMD" where ASE noise is neglected, "ASE" where PMD is not considered, and "ASE+PMD" when both ASE and PMD are present. It can be seen that the average EVM values for only PMD are much smaller than the values obtained for only ASE noise. However, PMD definitely affects the overall system performance because the EVM values including both PMD and noise are always larger than noise-only case. As expected, the average EVM increases for higher power or longer fiber. The linear filtering method has marginal effect on the PMD alone but significantly improves the performance in presence of ASE noise, with or without PMD. It can be observed in Table III that the difference between ASE+PMD and PMD increases when the ASE noise power increases (i.e., longer fiber length), and the impact of PMD becomes negligible compared to ASE. Likewise, the difference between ASE+PMD and ASE scales directly with the value of PMD parameter. For instance, compared to results in Table III in $L = 1000$ km and $P_{\mathrm{in}} = -6$ dBm, the EVM values are 12.17% and 11.52%, respectively for $D_{\mathrm{P}} = 0.8$ and $0.1\ \mathrm{ps}/\sqrt{\mathrm{km}}$ for ASE+PMD.

It can be seen in Table III that the average EVM squared for the ASE+PMD case is larger than the addition of the square of average EVMs for cases when only one of the effects exists. This implies that there is a correlation between the error originated from PMD and ASE in CS. Also, as explained in [20], an increase of noise power in time-domain is not linearly transformed to the noise added to CS. Note that the values shown in Table III are obtained including the pre-compensation of constellation rotation. As an example, without such compensation and any other modified detection according to the PMD induced phase shift, average EVMs are equal to 23.02 and 9.86, respectively for direct sampling and linear filtering, for $P_{in} = -6$ dBm and $L = 2000$ km for ASE+PMD. This happens because the EVM in this case is calculated considering original unrotated constellation points.

VI. Conclusions

The effect of PMD, as an inevitable phenomena in long-haul optical fiber communication, on the CS channel was studied. Due to the lack of an effective PMD compensation method that takes into account nonlinearity, an ideal linear PMD compensation method was exploited. It was demonstrated that, although most of the energy is returned to the original polarization using this method, the CS signal is affected by a residual polarization-dependent effect which is not compensated by the all-order linear PMD compensation method. A constellation rotation as well as a noise-like error was observed for the CS channel in simulations and was characterized based on a new perturbation model. The results show that for long-haul systems, at least a linear PMD compensation at the receiver should be included. Also, the constellation rotation can be precompensated at the transmitter side to further reduce the negative impact of PMD. In conclusion, the residual distortion remaining after linear PMD compensation is effectively negligible in our results although the highest level of PMD parameter is considered.

References

[1] J. C. Cartledge, F. P. Guiomar, F. R. Kschischang, G. Liga, and M. P. Yankov, "Digital signal processing for fiber nonlinearities," *Opt. Express*, vol. 25, no. 3, pp. 1916–1936, Feb. 2017.

[2] S. K. Turitsyn, J. E. Prilepsky, S. T. Le, S. Wahls, L. L. Frumin, M. Kamalian, and S. A. Derevyanko, "Nonlinear Fourier transform for optical data processing and transmission: advances and perspectives," *Optica*, vol. 4, no. 3, pp. 307–322, Mar. 2017.

[3] A. Ghazisaeidi, "A theory of nonlinear interactions between signal and amplified spontaneous emission noise in coherent wavelength division multiplexed systems," *J. Lightwave Technol.*, vol. 35, no. 23, pp. 5150–5175, Dec. 2017.

[4] M. Yousefi and F. Kschischang, "Information transmission using the nonlinear Fourier transform, part I: Mathematical tools," *IEEE Trans. Inf. Theory*, vol. 60, no. 7, pp. 4312–4328, Jul. 2014.

[5] ——, "Information transmission using the nonlinear Fourier transform, part II: Numerical methods," *IEEE Trans. Inf. Theory*, vol. 60, no. 7, pp. 4329–4345, Jul. 2014.

[6] ——, "Information transmission using the nonlinear Fourier transform, part III: Spectrum modulation," *IEEE Trans. Inf. Theory*, vol. 60, no. 7, pp. 4346–4369, Jul. 2014.

[7] A. Hasegawa and T. Nyu, "Eigenvalue communication," *J. Lightwave Technol.*, vol. 11, no. 3, pp. 395–399, Mar. 1993.

[8] I. Tavakkolnia and M. Safari, "Signaling on the continuous spectrum of nonlinear optical fiber," *Opt. Express*, vol. 25, no. 16, pp. 18 685–18 702, Aug. 2017.

[9] S. T. Le, J. E. Prilepsky, and S. K. Turitsyn, "Nonlinear inverse synthesis for high spectral efficiency transmission in optical fibers," *Opt. Express*, vol. 22, no. 22, pp. 26 720–26 741, Nov. 2014.

[10] T. Gui, C. Lu, A. P. T. Lau, and P. K. A. Wai, "High-order modulation on a single discrete eigenvalue for optical communications based on nonlinear Fourier transform," *Opt. Express*, vol. 25, no. 17, pp. 20 286–20 297, Aug. 2017.

[11] S. Hari, M. I. Yousefi, and F. R. Kschischang, "Multieigenvalue communication," *J. Lightwave Technol.*, vol. 34, no. 13, pp. 3110–3117, Jul. 2016.

[12] I. Tavakkolnia, A. Alvarado, and M. Safari, "Capacity estimates of single soliton communication," in *Proc. Eur. Conf. Opt. Commun.*, Sep. 2018, pp. 1–3.

[13] N. A. Shevchenko, S. A. Derevyanko, J. E. Prilepsky, A. Alvarado, P. Bayvel, and S. K. Turitsyn, "Capacity lower bounds of the noncentral Chi-channel with applications to soliton amplitude modulation," *IEEE Trans. Commun.*, vol. 66, no. 7, pp. 2978–2993, Jul. 2018.

[14] I. Tavakkolnia and M. Safari, "Signalling over nonlinear fibre-optic channels by utilizing both solitonic and radiative spectra," in *Proc. Eur. Conf. Netw. Commun.*, Jun. 2015, pp. 103–107.

[15] V. Aref, S. T. Le, and H. Buelow, "Modulation over nonlinear Fourier spectrum: Continuous and discrete spectrum," *J. Lightwave Technol.*, vol. 36, no. 6, pp. 1289–1295, Mar. 2018.

[16] S. T. Le, V. Aref, and H. Buelow, "Nonlinear signal multiplexing for communication beyond the Kerr nonlinearity limit," *Nature Photon.*, vol. 11, no. 9, pp. 570–577, Sep. 2017.

[17] ——, "High speed precompensated nonlinear frequency-division multiplexed transmissions," *J. Lightwave Technol.*, vol. 36, no. 6, pp. 1296–1303, Mar. 2018.

[18] H. Bülow, "Experimental demonstration of optical signal detection using nonlinear Fourier transform," *J. Lightwave Technol.*, vol. 33, no. 7, pp. 1433–1439, Apr. 2015.

[19] S. A. Derevyanko, J. E. Prilepsky, and S. K. Turitsyn, "Capacity estimates for optical transmission based on the nonlinear Fourier transform," *Nature Commun.*, vol. 7, pp. 1–8, Sep. 2016.

[20] I. Tavakkolnia and M. Safari, "Capacity analysis of signaling on the continuous spectrum of nonlinear optical fibers," *J. Lightwave Technol.*, vol. 35, no. 11, pp. 2086–2097, Jun. 2017.

[21] I. T. Lima, T. D. DeMenezes, V. S. Grigoryan, M. O'sullivan, and C. R. Menyuk, "Nonlinear compensation in optical communications systems with normal dispersion fibers using the nonlinear Fourier transform," *J. Lightwave Technol.*, vol. 35, no. 23, pp. 5056–5068, Dec. 2017.

[22] S. Civelli, E. Forestieri, and M. Secondini, "Why noise and dispersion may seriously hamper nonlinear frequency-division multiplexing," *IEEE Photon. Technol. Lett.*, vol. 29, no. 16, pp. 1332–1335, Aug. 2017.

[23] S. T. Le, J. E. Prilepsky, P. Rosa, J. D. Ania-Castanon, and S. K. Turitsyn, "Nonlinear inverse synthesis for optical links with distributed Raman amplification," *J. Lightwave Technol.*, vol. 34, no. 8, pp. 1778–1786, Apr. 2016.

[24] M. Kamalian, J. E. Prilepsky, S. T. Le, and S. K. Turitsyn, "On the design of NFT-based communication systems with lumped amplification," *J. Lightwave Technol.*, vol. 35, no. 24, pp. 5464–5472, Dec. 2017.

[25] I. Tavakkolnia and M. Safari, "Dispersion pre-compensation for NFT-based optical fiber communication systems," in *Proc. Conf. Lasers ElectroOpt.* Optical Society of America, Jun. 2016, p. SM4F4.

[26] ——, "Efficient signalling on the continuous spectrum of nonlinear optical fibre," in *Proc. Conf. Lasers ElectroOpt. Eur., Eur. Quantum Electron. Conf.*, Jun. 2017, p. CI_1_2.

[27] J.-W. Goossens, M. I. Yousefi, Y. Jaouën, and H. Hafermann, "Polarization-division multiplexing based on the nonlinear Fourier transform," *Opt. Express*, vol. 25, no. 22, pp. 26 437–26 452, Jul. 2017.

[28] S. Civelli, S. K. Turitsyn, M. Secondini, and J. E. Prilepsky, "Polarization-multiplexed nonlinear inverse synthesis with standard and reduced-complexity NFT processing," *Opt. Express*, vol. 26, no. 13, pp. 17 360–17 377, Jun. 2018.

[29] A. Maruta and Y. Matsuda, "Polarization division multiplexed optical eigenvalue modulation," in *Int. Conf. Photon. Switch. (PS)*, Sep. 2015, pp. 265–267.

[30] S. Gaiarin, A. M. Perego, E. P. da Silva, F. Da Ros, and D. Zibar, "Dual-polarization nonlinear Fourier transform-based optical communication system," *Optica*, vol. 5, no. 3, pp. 263–270, Mar. 2018.

[31] S. Gaiarin, F. D. Ros, N. D. Renzis, E. P. da Silva, and D. Zibar, "Dual-polarization nfdm transmission using distributed raman amplification and nft-domain equalization," *IEEE Photon. Technol. Lett.*, vol. 30, no. 22, pp. 1983–1986, Nov. 2018.

[32] X. Yangzhang, D. Lavery, P. Bayvel, and M. I. Yousefi, "Impact of perturbations on nonlinear frequency-division multiplexing," *J. Lightwave Technol.*, vol. 36, no. 2, pp. 485–494, Jan. 2018.

[33] I. Tavakkolnia and M. Safari, "Effect of PMD on the continuous spectrum of nonlinear optical fibre," in *Proc. Conf. Lasers ElectroOpt. Eur., Eur. Quantum Electron. Conf.*, Jun. 2017, p. CI_P_11.

[34] G. P. Agrawal, *Nonlinear fiber optics*, 5th ed. Academic Press, 2013.

[35] R. Essiambre, G. Kramer, P. J. Winzer, G. J. Foschini, and B. Goebel, "Capacity limits of optical fiber networks," *J. Lightwave Technol.*, vol. 28, no. 4, pp. 662–701, Feb. 2010.

[36] M. J. Ablowitz, B. Prinari, and A. D. Trubatch, *Discrete and continuous nonlinear Schrödinger systems*. Cambridge University Press, 2004.

[37] A. Shabat and V. Zakharov, "Exact theory of two-dimensional self-focusing and one-dimensional self-modulation of waves in nonlinear media," *Soviet Phys. JETP*, vol. 34, no. 1, p. 62, Jan. 1972.

[38] S. Hari and F. R. Kschischang, "Bi-directional algorithm for computing discrete spectral amplitudes in the NFT," *J. Lightwave Technol.*, vol. 34, no. 15, pp. 3529–3537, Aug. 2016.

[39] S. Wahls and H. V. Poor, "Fast numerical nonlinear Fourier transforms," *IEEE Trans. Inf. Theory*, vol. 61, no. 12, pp. 6957–6974, Dec. 2015.

[40] M. I. Yousefi and X. Yangzhang, "Nonlinear frequency-division multiplexing," *arXiv preprint arXiv:1603.04389*, 2016.

[41] V. Vaibhav, "Higher order convergent fast nonlinear Fourier transform," *IEEE Photon. Technol. Lett.*, vol. 30, no. 8, pp. 700–703, Apr. 2018.

[42] S. Wahls and V. Vaibhav, "Fast inverse nonlinear Fourier transforms for fiber Bragg grating design and related problems," *arXiv preprint arXiv:1607.01305*, 2016.

[43] C. Xie, M. Karlsson, P. A. Andrekson, H. Sunnerud, and J. Li, "Influences of polarization-mode dispersion on soliton transmission systems," *EEE J. Sel. Topics Quantum Electron.*, vol. 8, no. 3, pp. 575–590, May 2002.

[44] D. Marcuse, C. Manyuk, and P. Wai, "Application of the Manakov-PMD equation to studies of signal propagation in optical fibers with randomly varying birefringence," *J. Lightwave Technol.*, vol. 15, no. 9, pp. 1735–1746, Sep. 1997.

[45] C. R. Menyuk and B. S. Marks, "Interaction of polarization mode dispersion and nonlinearity in optical fiber transmission systems," *J. Lightwave Technol.*, vol. 24, no. 7, p. 2806, Jul. 2006.

[46] H. Sunnerud, C. Xie, M. Karlsson, R. Samuelsson, and P. A. Andrekson, "A comparison between different PMD compensation techniques," *J. Lightwave Technol.*, vol. 20, no. 3, p. 368, Mar. 2002.

[47] E. Ip, A. P. T. Lau, D. J. Barros, and J. M. Kahn, "Coherent detection in optical fiber systems," *Opt. Express*, vol. 16, no. 2, pp. 753–791, Jan. 2008.

[48] M. Safari and A. A. Shishegar, "Analysis of degree of polarization as a control signal in PMD compensation systems aided by polarization scrambling," *J. Lightwave Technol.*, vol. 26, no. 16, pp. 2865–2872, Aug. 2008.

[49] R. Balakrishnan, "Soliton propagation in nonuniform media," *Phys. Rev. A*, vol. 32, no. 2, p. 1144, Aug. 1985.